Analysis of dynamic effects in a rotary kiln system used for iron production

D.J. van Dyk [1] and **L. Pretorius** [2]

(First received June 1994; Final version December 1994)

Abstract

In this article a rotary kiln used in the iron manufacturing industry is modelled by means of two mathematical models. The macro model simulates the dynamic behaviour of the electric drive, burden and kiln. The micro model is used for a detail analysis of the drive train of the rotary kiln with emphasis on the girth gear and pinion in contact. Both models have been verified with the experimental results.

Nomenclature

Symbols

B_m	viscous friction coefficient [N.s.m/rad]
c_{po}	equivalent damping constant [N.s.m/rad]
e_f	difference signal [r.p.m.]
e_v	Reference signal [r.p.m.]
F_{bf}	breakout force [N]
F_t	tangential force of burden weight [N]
F_{ov}	spring force of girth gear teeth [N]
F_{pv}	spring force of pinion gear teeth [N]
F_{pb}	damping force of pinion gear teeth [N]
F_w	friction force [N]
g	gravitational constant [m/s^2]
i_a	armature current [amp]
J_e	$J_o + J_v$ [kg.m^2]
J_m	inertia of motor [kg.m^2]
J_o	inertia of kiln [kg.m^2]
J_v	inertia of burden [kg.m^2]
K	feedback constant [r.p.m.s/rad]
k	torque arm of bearing [m]
k_e	equivalent spring constant [N/m]
k_o	spring constant of girth gear teeth[N/m]
k_{pi}	spring constant of pinion gear teeth [N/m]
k_{po}	equivalent spring constant [N.m/rad]
k_p	proportional constant
k_D	derivative constant
k_I	integrational constant
k_b	k_i
k_i	torque constant [N.m/r.p.m.]
L	torque arm of burden [m]
l	torque arm of bearing [m]
L_a	armature inductance [H]
m_v	mass of burden [kg]
n	total reduction
P	total weight of kiln [N]
R	radius of kiln [m]
R_a	armature resistance [ohm]
R_o	pitch circle radius of girth gear [m]
R_p	pitch circle radius of pinion [m]
T	friction torque in bearing [N.m]
TFK	torque transmitted by coupling[N.m]
T_l	load [N.m]
T_m	motor torque [N.m]
T_o	torque on kiln [N.m]
T_p	torque on pinion [N.m]
W_t	tangential force transmitted by gears [N]
x_p	linear displacement of pinion teeth [m]
x_o	linear displacement of girth gear teeth [m]

Greek

Δx	backlash [mm]
θ_m	angular displacement of motor [rad]
θ_o	angular displacement of kiln [rad]
θ_p	angular displacement of pinion[rad]
μ	friction coefficient of burden
μ_{brg}	coefficient of friction of support roller bearing
μ_c	Coulomb friction coefficient
μ_s	static friction coefficient
ω_m	angular velocity of motor [rad/s]
Φ	angular displacement of burden[rad]

Introduction

Rotary kilns are widely used in production of cement, iron, etc. In this paper the authors concentrate on rotary kilns used in the iron production industry. The rotary kiln is a horizontal circular tube lined with refractory material, supported by support stations and driven via a girth gear and drive train. The drive train consists of two DC electrical motors and two high reduction gearboxes.

Several models are found in the literature modelling the retention time of the burden inside the kiln [1,2] as well as models for several possible ways of heat transfer.[3,4] Only similar dynamic models of ball mill drives [5] and refinery drives [6] are found.

[1]Post-graduate student. Rand Afrikaans University.

[2]Professor, Department of Mechanical Engineering, Rand Afrikaans University.

The maintenance of rotary kilns, especially the girth gear and drive train, is a very important aspect for the plant operations personnel, especially regarding the financial aspect and availability of spare parts. If the plant personnel understand the dynamic aspects of rotary kilns, their decision-making process will be easier.

The purpose of this study was to simulate the effect of several operating conditions on the dynamic aspects of rotary kilns. Operating conditions such as varying friction coefficient of the refractory lining, different feed rates and varying backlash between the girth gear and pinion were studied.

Mathematical model of the rotary kiln

The rotary kiln is modelled from two perspectives, respectively, namely a macro model and a micro model. A computer simulation language ACSL, Advanced Continuous Simulation Language, is used for the numerical simulation. The reasons for the two different models are (a) less computer time, and (b) for parametric studies to determine the coefficient of friction of the refractory lining.

The macro model is a model of the rotary kiln, burden and electric motor studying only macroscopic effects and thus a bigger integration step size is used in numerical simulations. The experimentally determined coefficient of friction of the refractory lining had to be verified with the macro model before it could be used in the more detailed micro model.

The study thus consists of two models where the results from the one simulation are used in the micro model numerical simulation, where short time effects are more important.

Development of the macro model

The macro model is a mathematical model of the kiln, burden inside the kiln, and the electrical motor. This model simulates the interaction of the burden inside the kiln with the kiln wall. The interaction between the pinion and the girth gear is not simulated and the gearbox is modelled as a pure torque reducer. The kiln is modelled as if driven directly by only one electrical motor. See Figure 1. The interaction between the two electric motors is thus disregarded.

During start up conditions of the kiln, the burden tends to stick to the kiln wall until the angle through which the kiln is turned is such that the angle of repose of the material is overcome. At this time the burden tumbles over and repeats the tumbling process during the rotation of the kiln. Although the burden follows a tumbling effect, it is modelled as a rigid disk similar to the shape of the burden. During the start up, two conditions prevail, namely (i) stick, and (ii) tumbling. The tumbling condition is modelled as if the burden effectively slides against the kiln wall.

The stick condition will prevail as long as the tangential force of the burden weight (F_t) is smaller than the breakout force (F_{bf}).

$$F_t = m_v g \sin(\pi - \Phi) \tag{1}$$

$$F_{bf} = \mu_s m_v g \cos(\pi - \Phi) \tag{2}$$

While the tangential force is smaller than the breakout force, a friction force (F_w) with the same magnitude as the tangential force but opposite in direction will keep the burden from slipping.

If the tangential force overcomes the breakout force, the friction force will be dominated by a Coulomb friction coefficient, thus permitting the burden to slip. The friction force will thus adhere to the following conditions:

$$\begin{array}{rcll} F_w & = & -F_t & F_t \leq F_{bf} \\ F_w & = & \mu_c m_v g \cos(\pi - \Phi) & F_t > F_{bf} \end{array} \tag{3}$$

From the above it is evident that two conditions will prevail. In the first stick condition, only one degree of freedom exists namely the burden, kiln and motor together. With the second condition slip, two degrees of freedom exist. The burden being one and the kiln and electrical motor being the other.

Stick condition

From Figure 1 and Euler's equations of motion [7] the differential equations are derived. The following equation of motion holds for the electrical motor:

$$T_m = J_m \ddot{\theta}_m + T_l \tag{4}$$

For the kiln it follows that:

$$T_o = J_o \ddot{\theta}_o + F_w R \tag{5}$$

and for the burden it follows that:

$$F_w R = -J_v \ddot{\Phi} + F_t L \tag{6}$$

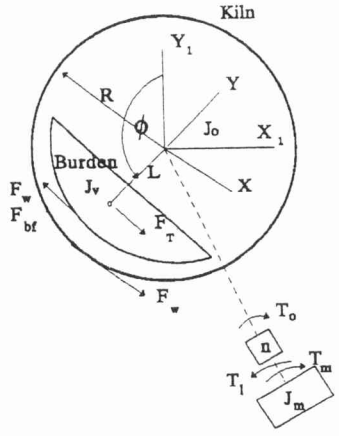

Figure 1 Kiln, burden and drive train

With the stick condition only one degree of freedom prevails, thus:

$$\theta_o = -\Phi \tag{7}$$

From equations (5) and (6) it.follows that:

$$T_o = J_o\ddot{\theta}_o + J_v\ddot{\theta}_o + F_tL \tag{8}$$

If

$$\begin{aligned} T_l &= \tfrac{1}{n}T_o \\ \theta_o &= \theta_m\tfrac{1}{n} \end{aligned} \tag{9}$$

it is derived from equation (8) that:

$$T_l = \frac{1}{n^2}(J_o + J_v)\ddot{\theta}_m + \frac{1}{n}F_tL \tag{10}$$

From equations (4) and (10) the differential equation describing the motion of the kiln with zero slip can be derived.

$$T_m = \left[J_m + \frac{1}{n^2}(J_o + J_v)\right]\ddot{\theta}_m + \frac{1}{n}F_tL \tag{11}$$

Slip condition

When the burden slips along the kiln wall, two degrees of freedom prevail. From Figure 1 the equations of motion for the first degree of freedom are derived.

$$T_m = J_m\ddot{\theta}_m + T_l \tag{12}$$

and

$$T_o = J_o\ddot{\theta}_o + F_wR \tag{13}$$

The degree of freedom of the electric motor and kiln being the same, it follows that:

$$\theta_o = \frac{1}{n}\theta_m \tag{14}$$

The equation of motion of the kiln and electric motor can thus be derived from equations (12), (13), and (14).

$$\begin{aligned} T_l &= \tfrac{1}{n^2}J_o\ddot{\theta}_m + \tfrac{1}{n}F_wR \\ T_m &= \left(J_m + \tfrac{1}{n^2}J_o\right)\ddot{\theta}_m + \tfrac{1}{n}F_wR \end{aligned} \tag{15}$$

The equation of motion of the second degree of freedom being that of the burden, is derived as follows:

$$\begin{aligned} F_wR &= -J_v\ddot{\Phi} + F_tL \\ F_w &= \mu_c m_v g\cos(\pi - \Phi) \\ F_T &= m_v g\sin(\pi - \Phi) \end{aligned} \tag{16}$$

The above mentioned equations hold for zero friction torque in the support rollers.

To accommodate the friction torque in the support roller bearings, the rotary kiln is.modelled as if it is supported by only two support roller bearings. Equation (17) describes the friction torque in the support roller bearings.[9]

$$T = 2\mu_{brg}\frac{P}{2}\cos 30°\left(\frac{l+k}{2}\right) \tag{17}$$

From the literature Le Roux [10] found the friction coefficient (μ_{brg}) to be 0.001

Equations (11) and (15) describing the motion of the kiln for the two different conditions including friction torque thus reduce to:

$$T_m = \left[J_m + \frac{1}{n^2}(J_o + J_v)\right]\ddot{\theta}_m + \frac{1}{n}F_tL + \frac{1}{n}T \tag{18}$$

or

$$T_m = \left(J_m + \frac{1}{n^2}J_o\right)\ddot{\theta}_m + \frac{1}{n}F_wR + \frac{1}{n}T \tag{19}$$

respectively.

Modelling of the electrical motor

Two DC electrical motors are used to drive the rotary kiln. For the purpose of this study the kiln is modelled as if driven by only one electrical motor. The purpose of the model is only to simulate an equivalent drive and control system and not the actual control system precisely. Figure 2 is a schematic diagram of a DC motor used to model the electrical drive of the rotary kiln.[8]

The motor speed is controlled between 100 r.p.m. and 1 000 r.p.m. by controlling the armature voltage. The optimum operating speed is at 500 r.p.m.. The differential equations of the motion of the motor without a feedback control is derived from Figure 2.[8]

$$\begin{aligned} \dot{i}_a &= \tfrac{1}{L_a}e_a - \tfrac{R_a}{L_a}i_a - \tfrac{K_b}{L_a}\omega_m \\ \dot{\omega}_m &= \tfrac{k_i}{J_m}i_a - \tfrac{T_l}{J_m} - \tfrac{B_m}{J_m}\omega_m \end{aligned} \tag{20}$$

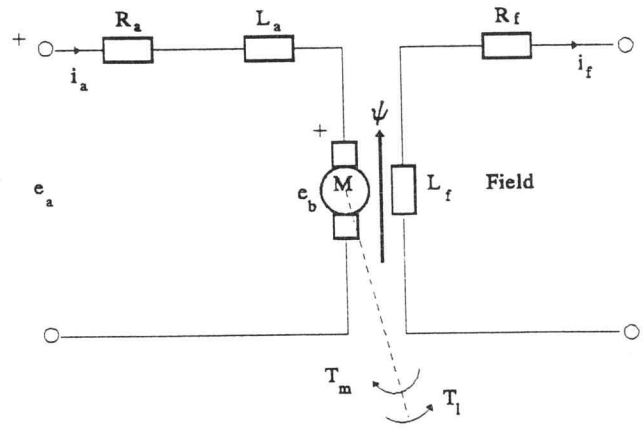

Figure 2 Direct current electric motor

The equivalent controller used is a PID controller that uses the output speed of the motor to compare to the reference speed set by the kiln operator. The PID controller

ensures minimum rise time with minimum over shoot in order not to induce vibrations in the modelled drive system. P, PI, and PD equivalent controllers have been modelled but the results were not satisfactory.

From Figure 2 a signal diagram is constructed for the internal control on the motor, which is modified to accommodate the equivalent external control on the motor. The result is shown in Figure 3.

From Figure 3 and Mason's gain formula,[8] the transfer function of the motor and PID controller can be derived. The control constants in the PID controller are determined from the characteristic equation of the transfer function. From the characteristic equation root loci are constructed in order to determine the constants k_p, k_D and k_I.

With the control constants known the equations of motion are determined from Figure 3.

$$\begin{aligned} \dot{i}_a &= \tfrac{1}{L_a} e_a - \tfrac{R_a}{L_a} i_a - \tfrac{k_b}{L_a} \dot{\theta}_m \\ i_a &= \int \dot{i}_a dt + \tfrac{k_D}{L_a} e_f \\ \ddot{\theta}_m &= \tfrac{k_i}{J_m} i_a - \tfrac{B_m}{J_m} \dot{\theta}_m - \tfrac{T_l}{J_m} \\ \dot{\theta}_m &= \int \ddot{\theta}_m dt \\ e_a &= k_p e_f + k_I \int e_f dt \\ e_f &= e_v - k\dot{\theta}_m \end{aligned} \tag{21}$$

With the equations of motion of the kiln, burden and electrical motor known, the dynamic behaviour of the kiln can be simulated. In order to simulate the kiln and drive train, a numerical computer simulation language, ACSL is used. The differential equations are entered into ACSL in a fortran format before ACSL translates it via a fortran compiler.[9]

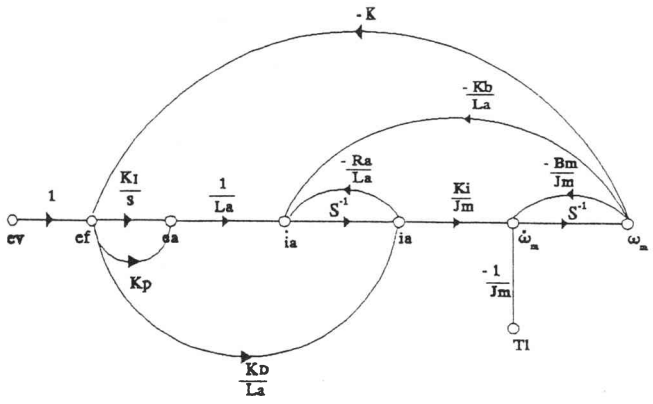

Figure 3 Signal flow diagram

Numerical results from the macro model simulation

The program flow diagram for the macro model is similar to that shown for the micro model in Figure 8. Typical values for the constants used in the numerical simulations for the macro and micro models are shown in Table 1. These values are typical for rotary kilns used in the iron manufacturing industry.

Table 1 Typical values used in the numerical simulations of the macro and micro model

Constant	Value
B_m	0.005
C_{po}	19.9×10^6
J_e	8.476×10^6
J_m	21.5
J_o	6.978×10^6
J_v	1.678×10^6
k	0.5475
k_o	2.986×10^{10}
k_{pi}	2.986×10^{10}
k_{po}	7.012×10^8
k_i	4.6
L	1.353
l	0.7155
L_a	0.57×10^{-3}
m_v	580×10^3
n	1076.5
P	16.512×10^6
R	2.17
R_a	0.00961
R_o	3.960
R_p	0.5775

During the simulation with the macro model, the effective friction coefficient between the burden and the kiln wall was not known. A parametric study was done by varying the friction coefficient and determining the motor current. The numerical results are then compared with the experimental results in order to find an effective friction coefficient. The motor current was used as a parameter for comparison purposes.

From the numerical results, Figure 4, the condition (mu3) for $\mu_c = 0.4$ and $\mu_s = 0.51$ was found to simulate the dynamic behaviour of the kiln the closest. From the experiment done, the burden was found to settle after 17 s at 650 ampere where it oscillates as shown in Figure 5. From the numerical simulation the burden took 15 s to settle at 620 ampere where it oscillates. The difference in the frequency of the oscillation depicted numerically and determined experimentally may be due to the following: (a) the exact mass of the burden during operation is unknown, (b) the exact condition of the kiln wall is unknown, and (c) the burden is not necessarily a rigid mass.

From Figure 5 a peak of 420 ampere can be seen at start up. The absence of this peak in Figure 4 is due to the fact that the simulation was done with only one electrical motor. The experiment was done with the second electrical motor isolated only electrically, and thus the inertia of the second motor has still to be overcome.

The oscillation can be verified with mathematical manipulation of equation (16).

$$J_v \ddot{\Phi}_1 = -C_1 \sin(\Phi_1) - c_2 \cos(\Phi_1) \tag{22}$$

with

$$\Phi = \Phi_1 + \pi \tag{23}$$

where

$$C_1 = m_v g L$$
$$C_2 = \mu_c m_v g R$$

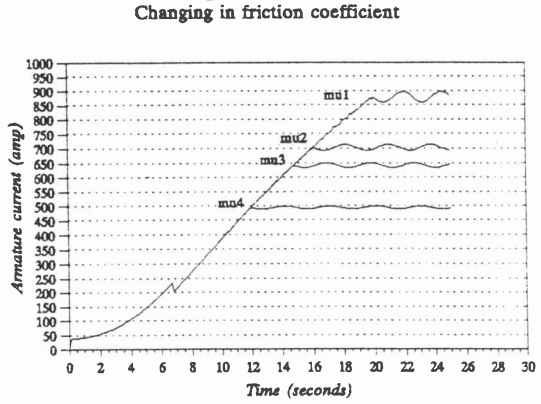

Figure 4 Stabilizing of the motor current

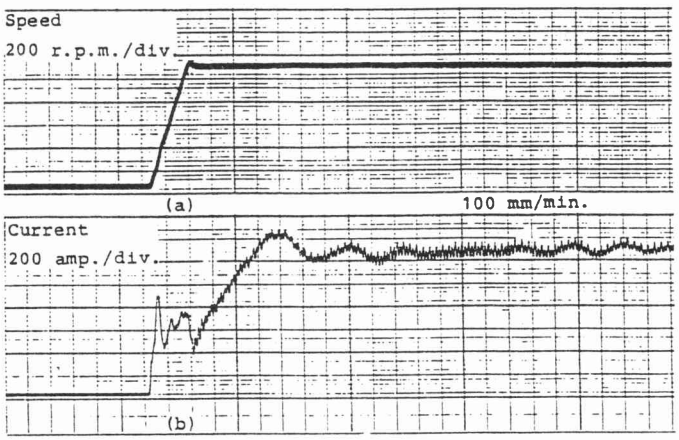

Figure 5 Motor current determined experimentally

For small oscillations of the burden it can be assumed that:

$$\begin{aligned} \sin \Phi_1 &\approx \Phi_1 \\ \cos \Phi_1 &\approx 1 \end{aligned} \tag{24}$$

When equation (24) is substituted in equation (22) it follows that:

$$J_v \ddot{\Phi}_1 = -C_1 \Phi_1 - C_2 \tag{25}$$

The burden behaves like a system with zero damping that oscillates about a fixed position.

Development of the micro model

The macro model was verified successfully with the experimental results and the effective friction coefficient of friction of the refractory lining determined parametrically as shown in the previous paragraph. The model was developed further to accommodate the backlash between the girth gear an pinion, stiffnesses of the gears and the nonlinear elastomeric coupling between the electric motor and gearbox, with the intention of studying short time transients.

Figure 6 is a schematic diagram of the micro model which is a more detailed portrayal of the drive train of the rotary kiln.

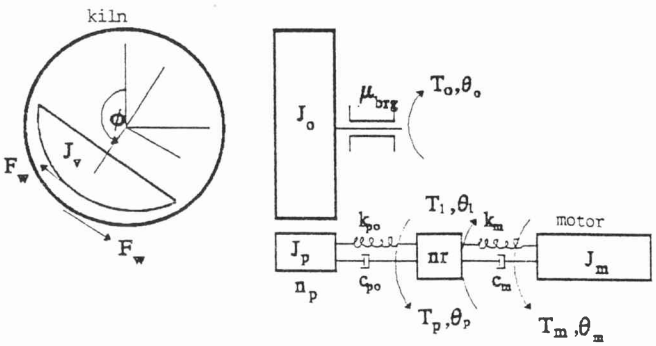

Figure 6 Schematic diagram of the micro model

Modelling of the gear teeth in contact

With the modelling of the girth gear and pinion in contact the backlash was also taken into account. The stiffnesses of the gear teeth, girth gear, and pinion are assumed to be the same and the stiffness of the pinion shaft is included into the stiffness of the gears.

It is also assumed that the stiffness of the gear during contact stays constant. The variation in stiffness during contact was taken into account by varying the line of contact as developed by Michalopoulos.[11] From Figure 7 the equations of motion can be derived.

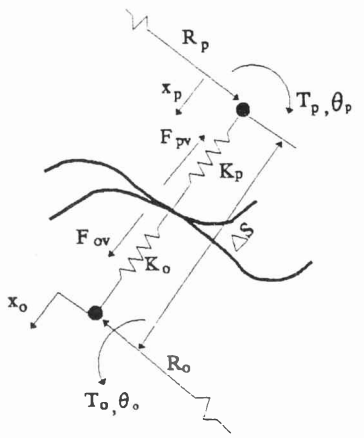

Figure 7 Schematic diagram of two gears in contact

When the two gears are in contact the two springs k_o, and k_{pi}, are physically in series. The equivalent spring is described by equation (26):

$$K_e = \frac{K_o K_{pi}}{Ko + K_{pi}} \tag{26}$$

The force that is transmitted by the gears when in contact are determined by equation (27):

$$F_{pv} = -K_e \Delta s \tag{27}$$

where

$$\Delta s = (R_p \theta_p - R_o \theta_o)$$

If the reduction ratio between the girth gear and pinion is designated by n_p and the backlash assumed to be zero, then it follows that:

$$F_{pv} = -K_e R_p (\theta_p - n_p \theta_o) \tag{28}$$

where

$$R_o = n_p R_p$$

The torque that is transmitted by the pinion can be computed from equation (29) for the stiffness and equation (30) for the damping:

$$\begin{aligned} T_{pv} &= -F_{pv} R_p \\ &= -K_e {R_p}^2 (\theta_p - n_p \theta_o) \end{aligned} \tag{29}$$

$$T_{pb} = -C_e {R_p}^2 \left(\acute{\theta}_p - n_p \acute{\theta}_o\right) \tag{30}$$

If a backlash of Δs does exist between the gear teeth, the force transmitted between the girth gear and pinion is transferred according to the following conditions:[11]

$$\begin{gathered} 0 < \Delta s < \Delta x \\ F_{pv} = 0 \end{gathered}$$

if

$$\begin{gathered} \Delta s > \Delta x \\ F_{pv} = -K_e R_p (\theta_p - n_p \theta_o - \Delta x) \end{gathered} \tag{31}$$

if

$$\begin{gathered} \Delta s < 0 \\ F_{pv} = -K_e R_p (\theta_p - n_p \theta_o) \end{gathered}$$

The same conditions can be derived for the force transmitted due to damping. The total tangential force transmitted by the girth gear and pinion can thus be computed from:

$$W_t = F_{pv} + F_{pb} \tag{32}$$

where F_{pv} is determined by equation (31) and F_{pb} an equation similar to (31).

The differential equations describing the gear pair can thus be derived. With the assumption that the burden sticks to the kiln wall during start up conditions, it follows from Figure 6 and Figure 7 that:

$$T_p = J_p \ddot{\theta}_p + W_t R_p \tag{33}$$

and

$$W_t R_o = J_e \ddot{\theta}_o + T_o \tag{34}$$

The gear pair is connected to the electrical motor via a reduction gearbox with a reduction ratio of n_r and a non-linear elastomeric coupling. The non-linear effects on the torque transmitted by the coupling are induced in the micro model. Details of this are included in [9]. The reduction gearbox is modelled as a pure torque reducer.

Numerical results from the simulation

Having established the differential and other equations for the micro model, they are programmed .in ACSL in a similar procedure as for the macro model.[9] Figure 8 is a program flow diagram for the micro model.

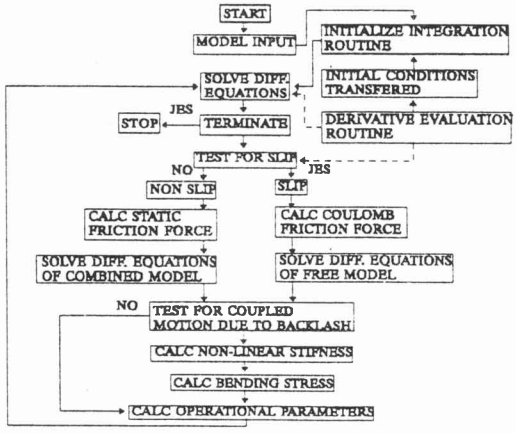

Figure 8 ACSL program flow diagram for the micro model

As a first verification the movement of the burden inside the kiln was studied. With the kiln fixed the burden is simulated as a pendulum falling free through gravitation. From Figure 9 it is evident that the motion of the burden is characteristic of a body subject to Coulomb friction. With a Coulomb coefficient of friction of $\mu_c = 0.35$ and a static coefficient of friction of $\mu_s = 0.38$, the burden took 10 s to settle down to an offset from the zero mark.

Figure 10 shows the numerical results obtained from the micro model during start up of the rotary kiln. Graph A represents the motor current while graph B represents the motor speed. From Figure 10 it is evident that the motor current peaks at 280 ampere during the acceleration of the kiln. From the experimental study (Figure 6), a peak of 450 ampere is evident. The deviation is due to the inertia of the second electric motor which has to be overcome.

It can thus be seen that the micro model adequately simulates the effects gathered from experiments.

Parametric study

The micro model can be developed further to accommodate the computation of the bending stress in the gear teeth of the girth gear as developed by Michalopoulos.[11]

With the bending stress known a parametric study was done to study the influence of several operating conditions on an industrial application. Full details of the development are shown in [9].

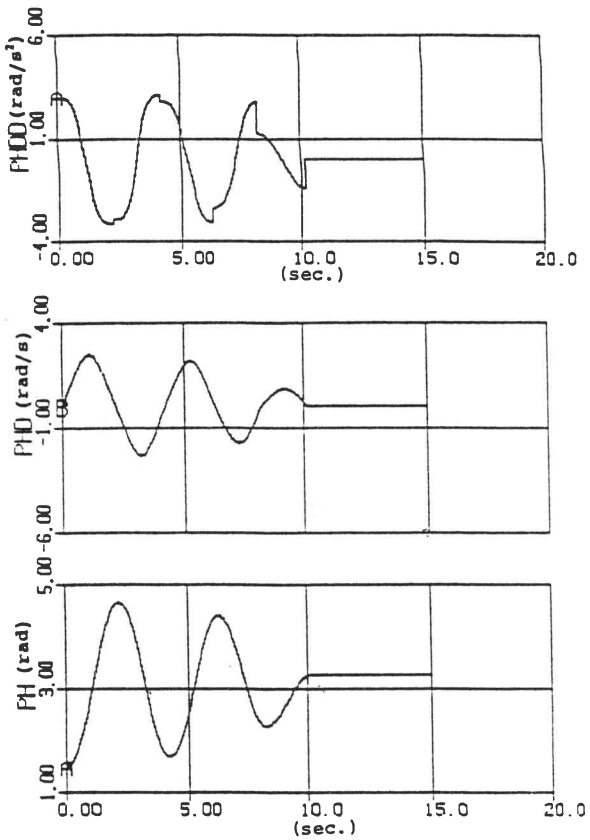

Figure 9 Motion of the burden with $\mu_c = 0.35$ and $\mu_s = 0.38$

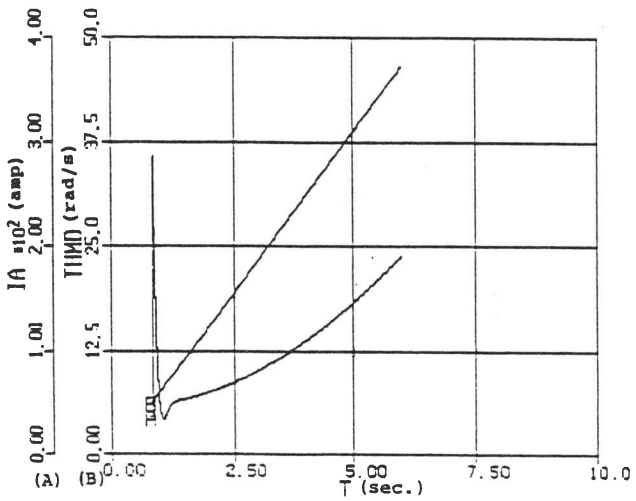

Figure 10 Numerical results from the micro model

The following operating conditions were studied: (a) influence of a varying backlash in gears during start up, (b) forming of accretions, and (c) varying the ramp generator of the controller on the electric motor.

During the operation of a rotary kiln the backlash changes due to the centre line of the kiln changing. The centre line of the kiln changes, due to temperature differences in the circumference varying, resulting in a permanent bend in the kiln shell. The parametric study was done with a backlash varying between 0 mm and 16 mm. During normal operating conditions a backlash of approximately 8 mm is maintained. Figure 11 shows a variation in stress for a varying backlash while Figure 12 shows a typical stress curve during start up for a backlash of 10 mm. All these values were calculated by the numerical simulation of the micro model.[9]

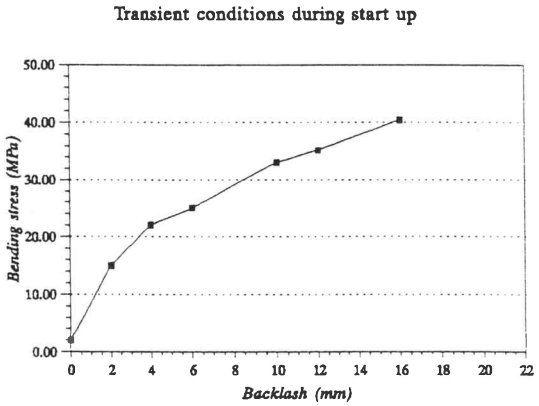

Figure 11 Varying the backlash during start up conditions

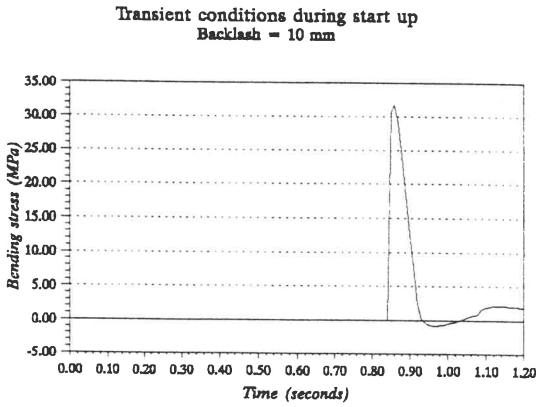

Figure 12 Typical stress curve for a transient condition at start up

Due to the process inside the rotary kiln and other contributing factors accretions tend to build up inside the kiln. These accretions form a ring on the kiln wall on the inside. Due to the accretions the material flow is restricted and thus the nett mass that has to be turned by the electric drive is larger. This effect was simulated by increasing the mass of the burden as well as the inertia in the micro model.

The variation of the inertia of the burden has a very small effect on the bending stress in the gear teeth during

start up (Figure 13). The variation of the burden mass has a significant influence on the stress in the gear teeth. The mass was increased parametrically from 240 000 kg to 974 000 kg. The stress is calculated after the transient conditions have died out and the burden has reached the optimum angle in the kiln. From Figure 14 it is evident that the mass of the burden is a critical factor in the operation of the rotary kiln. An increase in mass, of 100 %, increases the stress levels by 120 %.

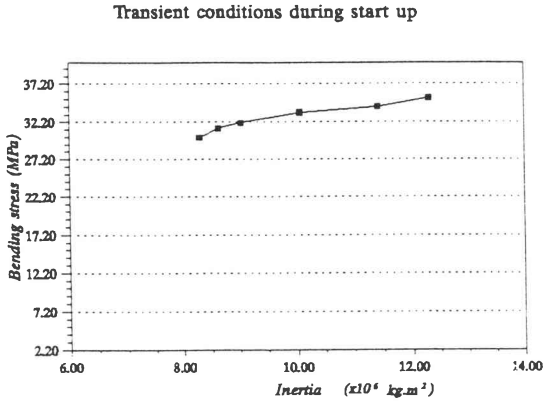

Figure 13 Varying inertia of the burden

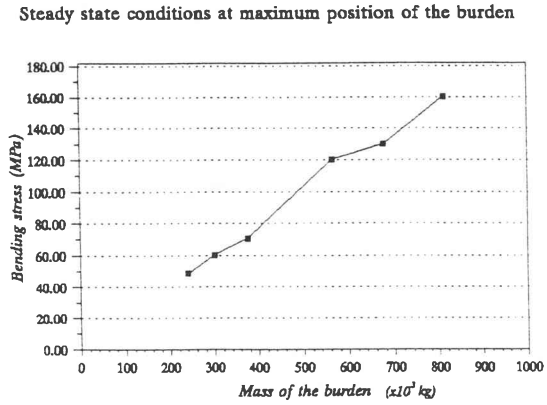

Figure 14 Varying the mass of the burden

During start up of the rotary kiln the current in the electrical drive is ramped by a certain ramp constant. The ramp constant ensures a smooth start up and acceleration. The influence of a varying ramp constant on the drive train was also studied. From Figure 15 it is evident that an increase of a factor of 10 on the ramp constant will increase the stress level by a factor of 4. A typical ramp constant used on a rotary kiln is 74.

Conclusion

The macro and micro model have been found to simulate the dynamic behaviour of the drive train of the rotary kiln adequately. From the parametric study it is evident that the operating condition where accretions are formed on the kiln wall must be avoided. The accretions have their largest influence on the stress during steady state operating conditions. No evidence of vibrations being excited by a varying backlash during start up could be found during calculations due to the slow speed of the gears prior to engagement. This result is expected.

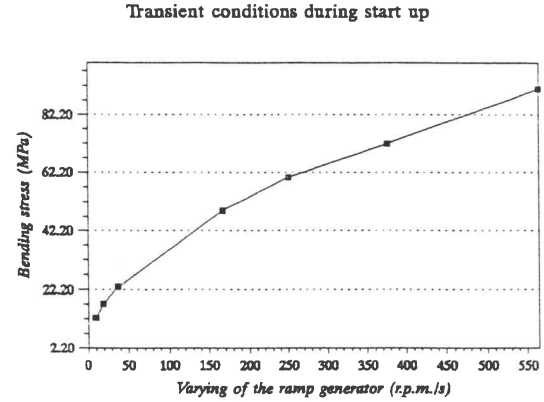

Figure 15 Varying the ramp generator during start up conditions

The mathematical model developed during this study can assist engineers, designing similar systems, as well as maintenance personnel of similar plants. The model can also be used to assist in the evaluation of a gearbox, electrical drive or coupling for rotary kiln systems.

References

[1] Chatterjee A, Sathe AV, Spirvastava MP & Mukhopadhyay PK. Flow of materials in rotary kilns used for sponge iron manufacture: Part I. Effect of some operational variables. *Metallurgical Transactions*, **14b**, 1983, 375–381.

[2] Sathe AV, Chatterjee A & Mukhopadhyay PK. Flow of materials in rotary kilns used for sponge iron manufacture: Part II. Effect of kiln geometry. *Metallurgical Transactions*, **14b**, 1983, 383–392.

[3] Barr PV, Brimacombe JK & Watkinson AAPHeat transfer model for the rotary kiln: Part 1. Pilot kiln trials. *Metallurgical Transactions*, **20b**, 1989, 91–401.

[4] Barr PV, Brimacombe JK & Watkinson AP. Heat transfer model for the rotary kiln: Part II. Development of the cross-section model. *Metallurgical Transactions*, **20b**, 1989, 403–419.

[5] Michalopoulos D, Aspragathos N & Dimarogonas AD. Analytical investigation of a turning gear mechanism during engagement due to stick-slip. *Mechanism and Machine Theory*, **12**, 1986, 145–151.

[6] Mayer CB. Torsional dynamics – An important consideration in large refiner drive systems. *Engineering Conference*, 1985, 105–115.

[7] Wells DA. *Lagrangian Dynamics.* Schaum Outline series. McGraw-Hill, 1974.

[8] Kuo BC. *Automatic Control Systems.* Fifth Edition. Prentice Hall International Editions, 1987.

[9] Van Dyk DJ. Dinamiese aspekte van draaioonde in ystervervaardiging. MEng thesis, Rand Afrikaans University, 1993.

[10] Le Roux HJ. Wringkragverspreiding in roterende elektromeganiese aandryfstelsels tydens dinamiese bedryfstoestande. DEng Thesis, Rand Afrikaans University, 1990.

[11] Michalopoulos D, Aspragathos N & Dimarogonas AD. Fatigue damage of gear teeth in speed reducers moving heavy rotors. *Transactions of ASME*, **109**, 1987, 196–200.